JOURNAL OF GEOPHYSICAL RESEARCH, VOL. 106, NO. C8, PAGES 16,711–16,728, AUGUST 15, 2001

Improving the utility of ocean circulation models through adjustment of the momentum balance

Jinyu Sheng and Richard J. Greatbatch
Department of Oceanography, Dalhousie University, Halifax, Nova Scotia, Canada

Daniel G. Wright
Fisheries and Oceans Canada, Bedford Institute of Oceanography, Dartmouth, Nova Scotia, Canada

Abstract. We propose a new method to improve the utility of three-dimensional ocean circulation models. The method uses climatological temperature and salinity data to adjust the momentum balance of the model, while leaving the tracer equations fully prognostic and unconstrained. The adjustment is accomplished by replacing density in the hydrostatic equation by a linear combination of model-computed and climatological density. The procedure is equivalent to adding a forcing term to the horizontal momentum equation through a modification of the model's horizontal pressure gradient term. The forcing term modifies the model-computed velocity field, which, in turn, affects the model-computed temperature and salinity fields through the advection term (there is no adjustment of the tracer equations carried by the model). Assuming the linear combination coefficient to be invariant in time and space, we suggest a statistical approach to estimating its optimal value. We apply this "semiprognostic" method to the northwest Atlantic. A primitive equation circulation model is initialized with January climatological temperature and salinity and is forced by monthly mean Comprehensive Ocean-Atmosphere Data Set surface wind stress and heat flux, by restoration of the surface salinity to monthly mean climatology, and by flows through the open boundaries. Both the model-computed tracer and velocity fields produced using the semiprognostic method show significant improvement over those produced by a purely prognostic calculation; drift of the tracer and velocity fields away from climatology is greatly reduced. Further, convective mixing is explicitly represented, thus improving the utility of results over those obtained from pure diagnostic calculations. The velocity fields obtained with the new approach are somewhat more realistic than those obtained from pure diagnostic calculations. The method reproduces many well-known circulation features in the region, including the Labrador Current, the Gulf Stream, and the North Atlantic Current. More significantly, the method reproduces reasonably well the seasonal evolution of temperature and salinity in the region despite the fact that the model's tracer fields are not constrained directly by the new method. This result suggests that the semiprognostic approach will be useful for examining the evolution of tracers that are not easily determined by observations.

1. Introduction

With increasing computer power and advances in computational fluid dynamics, ocean models are increasingly being used in prognostic mode to simulate ocean circulation and water mass properties. In such prognostic calculations the momentum equations, as well as the conservation equations for temperature and salinity, are integrated forward as an initial value problem, whereas in diagnostic calculations, ocean currents are calculated using temperature and salinity fields that are specified at all model grid points at each time step [*Blumberg and Mellor*, 1987]. Although prognostic calculations include more complete physics than diagnostic calculations, the simulation performance of a prognostic run is not necessarily always better than that of a diagnostic run. Indeed, it is often found that the skill of a prognostic run is worse than a diagnostic run, particularly in multiyear simulations. This is not totally unexpected since prognostic models contain a greater number of degrees of freedom than diagnostic models, and important processes such as internal mixing, bottom friction, and flows across steep topography are often not well represented. Furthermore, even a slight drift in water mass properties can influence the currents, and the subsequent feedbacks can result in unrealistic results as the effects accumulate over time.

In estimating three-dimensional ocean currents and volume transport from climatological temperature and salinity fields for the North Atlantic, *Sarmiento and Bryan* [1982] proposed a "robust diagnostic" method in which Newtonian damping terms are added to the conservation equations for temperature and salinity. In this approach the temperature and salinity fields are permitted to adjust dynamically but are constrained to remain near the observed climatology by the addition of artificial sources and sinks of heat and salt. Sarmiento and Bryan demonstrate the robustness of their method in the sense that the model results are less sensitive to errors in the input density field than those of a purely diagnostic calculation, while the drifts of the predicted temperature and salinity fields are

Paper number 2000JC000680.
0148-0227/01/2000JC000680$09.00

far less than those produced by a prognostic calculation. The main drawback of their method is the creation of unphysical internal buoyancy sources and sinks that violate the principles of heat and salt conservation.

Recent studies on mixing and transport by mesoscale eddies suggest that with appropriate interpretation of the model velocities the effects of eddies on tracer transport can be represented through the addition of forcing terms to the momentum equations [*Greatbatch and Lamb*, 1990; *Gent et al*., 1995; *Greatbatch*, 1998; *Wardle and Marshall*, 2000]. Also, *Holloway* [1992] and colleagues parameterized the effects of topographic stress through an additional term in the momentum equations. Motivated in part by these theoretical considerations and by our desire to nudge model results toward climatology without violating tracer conservation, we examine here the possibility of using climatological temperature and salinity data to modify the momentum equations in models in order to improve the model performance. The method differs from that suggested by *Woodgate and Killworth* [1997] in that we do not add relaxation terms directly in the momentum equations. Instead, we replace the conventional density term in the hydrostatic equation by a linear combination of model-computed and climatological density. The procedure is equivalent to adding a forcing term to the momentum equations by modifying the horizontal pressure gradient term seen by the model.

The plan of this paper is as follows. The basic governing equations are presented in section 2. Estimation of the linear combination coefficient using the statistical approach known as the best linear unbiased estimator is discussed in section 3. The application of this new method to the northwest Atlantic is given in section 4. A summary and discussion of results are presented in section 5.

2. Basic Governing Equations

The three-dimensional primitive equations for our model can be written in spherical coordinates as

$$\frac{\partial u}{\partial t} + \mathcal{L}u - \left(f + \frac{u \tan\phi}{R}\right) v = -\frac{1}{\rho_o R \cos\phi}\frac{\partial p}{\partial \lambda} + \mathcal{D}_m u + \frac{\partial}{\partial z}\left(K_m \frac{\partial u}{\partial z}\right), \tag{1}$$

$$\frac{\partial v}{\partial t} + \mathcal{L}v + \left(f + \frac{u \tan\phi}{R}\right) u = -\frac{1}{\rho_o R}\frac{\partial p}{\partial \phi} + \mathcal{D}_m v + \frac{\partial}{\partial z}\left(K_m \frac{\partial v}{\partial z}\right), \tag{2}$$

$$\frac{1}{R\cos\phi}\left[\frac{\partial u}{\partial \lambda} + \frac{\partial (v\cos\phi)}{\partial \phi}\right] + \frac{\partial w}{\partial z} = 0, \tag{3}$$

$$\frac{\partial p}{\partial z} = -[\alpha\rho_p + (1-\alpha)\rho_c]g, \tag{4}$$

$$\rho_p = \rho(T, S, p), \tag{5}$$

$$\rho_c = \rho(T_c, S_c, p), \tag{6}$$

$$\frac{\partial T}{\partial t} + \mathcal{L}T = \mathcal{D}_h T + \frac{\partial}{\partial z}\left(K_h \frac{\partial T}{\partial z}\right), \tag{7}$$

$$\frac{\partial S}{\partial t} + \mathcal{L}S = \mathcal{D}_h S + \frac{\partial}{\partial z}\left(K_h \frac{\partial S}{\partial z}\right), \tag{8}$$

where t is time; u, v, and w are the east (λ), north (ϕ), and vertical (z) components, respectively, of the velocity vector $\vec{\mathbf{u}}$; p is pressure (see below); ρ_p is the density calculated from the model potential temperature T and salinity S, which, in turn, are updated using the conservation equations defined in (7) and (8); ρ_c is the density calculated from climatological potential temperature T_c and salinity S_c; K_m and K_h are vertical eddy viscosity and diffusivity coefficients, respectively; f is the Coriolis parameter; ρ_o is a reference density; R and g are the Earth's radius and gravitational acceleration, respectively; L is an advection operator defined as

$$\mathcal{L}q = \frac{u}{R\cos\phi}\frac{\partial q}{\partial \lambda} + \frac{v}{R}\frac{\partial q}{\partial \phi} + w\frac{\partial q}{\partial z}, \tag{9}$$

where q is an arbitrary scalar; and $\mathcal{D}_m$ and $\mathcal{D}_h$ are diffusion operators defined as

$$\mathcal{D}_{(m,h)}q = \frac{A_{(m,h)}}{R^2}\left(\frac{1}{\cos^2\phi}\frac{\partial^2 q}{\partial \lambda^2} - \tan\phi\frac{\partial q}{\partial \phi} + \frac{\partial^2 q}{\partial \phi^2}\right), \tag{10}$$

where A_m and A_h are horizontal eddy viscosity and diffusivity coefficients, respectively.

The governing equations presented above are conventional [see *Sheng et al*., 1998] except for the term in brackets on the right side of the hydrostatic equation (equation (4)). Here the conventional density term is replaced by a linear combination of model-computed density ρ_p and climatological density ρ_c: $\alpha\rho_p + (1-\alpha)\rho_c = \rho_p + (1-\alpha)(\rho_c - \rho_p)$, where α is the linear combination coefficient with a value between 0 and 1 (see section 3). It is readily seen that if $\alpha = 1$, the ocean circulation model is purely prognostic, whereas if $\alpha = 0$, the model is purely diagnostic.

It is helpful to consider the following interpretation of our model equations. We first separate the pressure variable p into two parts:

$$p = p^* + \tilde{p}, \tag{11}$$

where

$$\frac{\partial p^*}{\partial z} = -\rho_p g \tag{12}$$

$$\frac{\partial \tilde{p}}{\partial z} = (1-\alpha)(\rho_c - \rho_p)g. \tag{13}$$

Note that p^* is obtained from (12) by relating its surface value to the sea surface elevation, as is traditionally done with the pressure variable in ocean models, while $\tilde{p}$ is obtained from (13) by putting $\tilde{p} = 0$ at the surface $z = 0$. Writing the horizontal momentum equations in terms of p^* and $\tilde{p}$, we obtain

$$\frac{\partial u}{\partial t} = -\frac{1}{\rho_o R\cos\phi}\frac{\partial p^*}{\partial \lambda} - \frac{1}{\rho_o R\cos\phi}\frac{\partial \tilde{p}}{\partial \lambda} + \text{others} \tag{14}$$

$$\frac{\partial v}{\partial t} = -\frac{1}{\rho_o R}\frac{\partial p^*}{\partial \phi} - \frac{1}{\rho_o R}\frac{\partial \tilde{p}}{\partial \phi} + \text{others}. \tag{15}$$

Viewed in this way, p^* corresponds to the traditional pressure variable carried by the model, since p^* satisfies the conventional hydrostatic equation and surface boundary condition. In fact, p^* corresponds to the physical pressure that would be measured in the ocean. In contrast, the terms involving $\tilde{p}$

appear as forcing terms in the model momentum equations, and it is these forcing terms that are responsible for modifying the model-computed velocities that, in turn, modify the tracers through the advection terms in (7) and (8). The forcing terms associated with $\tilde{p}$ can be thought of as representing unresolved processes and are analogous to the eddy forcing terms suggested by several authors [e.g., *Holloway*, 1992; *Greatbatch*, 1998], although their detailed form is different. Since the new method introduces forcing terms in the momentum equations, the method does affect the momentum and energy balance for the "mean flow" being computed by the model. It is implicit, however, that the momentum and energy budgets are closed by the unresolved scales of motion (or by processes that are not being correctly represented by the model equations).

It is important to note the differences between the method introduced here and the robust diagnostic method suggested by *Sarmiento and Bryan* [1982]. First, the new method introduces forcing terms into the model's momentum equations (the terms associated with $\tilde{p}$ above) but leaves the model temperature and salinity equations fully prognostic and unconstrained. The forcing terms modify the model-computed velocities, and these, in turn, affect tracers through the advection terms in the tracer equations; the method does not constrain the tracer equations directly in order to push the model's tracer fields toward observations. By contrast, Sarmiento and Bryan's method nudges the model-computed temperature and salinity toward climatology through Newtonian damping terms in their tracer conservation equations. Since the temperature and salinity equations are purely prognostic and unconstrained in the new approach, we refer to the new method as being "semiprognostic." It should also be noted that since the new method does not involve using a Newtonian damping term, the method does not introduce phase errors between the model-computed fields and climatology, as discussed by *Woodgate and Killworth* [1997] and *Pierce* [1996]. It remains to determine an appropriate value of α to use in the semiprognostic equations, an issue that is addressed in section 3.

3. Best Linear Unbiased Estimator

The linear combination coefficient α, in general, should be a function of time and space. For simplicity, here we consider α to be invariant in time and space and discuss an approach to estimating its value on the basis of the statistical approach known as the best linear unbiased estimator (BLUE).

BLUE is a simple statistical technique that is widely used for the objective analysis of atmospheric data [*Daley*, 1991]. The main idea of this technique can be described as follows. Let X_1 and X_2 be two unbiased estimates for a variable X_e with uncorrelated errors and error variances of σ_1^2 and σ_2^2, respectively. Any linear combination of the form $\alpha X_1 + (1 - \alpha)X_2$ is an unbiased linear estimate of X_e.

To estimate the optimal value of α, we minimize the cost function defined as [*Ghil*, 1989; *Daley*, 1991]

$$J = \frac{1}{2}\sum^{N}\left[\frac{1}{\phi_1^2}(X_e^* - X_1)^2 + \frac{1}{\sigma_2^2}(X_e^* - X_2)^2\right], \quad (16)$$

where $X_e^* = \alpha X_1 + (1 - \alpha)X_2$ and N is the total number of estimates of X_e at locations where observations were made. The resulting optimal value of α is then given by

$$\hat{\alpha} = \frac{\sigma_1^{-2}}{\sigma_1^{-2} + \sigma_2^{-2}} \equiv \frac{\sigma_2^2}{\sigma_1^2 + \sigma_2^2}. \quad (17)$$

It can readily be seen from (17) that $\hat{\alpha} \to 1$ in the case of $\sigma_1^2 \ll \sigma_2^2$ and $\hat{\alpha} \to 0$ in the case of $\sigma_1^2 \gg \sigma_2^2$. This reflects the fact that X_e is best approximated by X_1 if the error variance σ_1^2 is much smaller than σ_2^2, and X_e is best approximated by X_2 if the error variance σ_2^2 is much less than σ_1^2.

Note that the state variable X_e in (16) could be density, pressure, or velocity. In this paper we consider X_e to be monthly mean velocity field produced by the model at the locations where monthly mean current observations are available. X_1 and X_2 are the monthly mean velocity fields produced by the purely prognostic and purely diagnostic calculations, respectively (the estimation of σ_1^2 and σ_2^2 is discussed in section 4.3). The resulting estimate of α is appropriate to the optimal, direct combination of the purely prognostic and purely diagnostic results to obtain an estimate for the observed velocity field.

We use the above procedure to estimate the value of α for use in (4). If ρ_p in (4) were replaced with the estimates of ρ obtained from a purely prognostic run, then, provided we have a linear model including linear tracer as well as momentum equations, our approach would be a simple linear blending of the pure prognostic and pure diagnostic runs, and $\hat{\alpha}$ would be very near the optimal choice. However, not only is our model nonlinear, but the ρ_p used in (4) is actually the model estimate of ρ obtained with $\alpha = \hat{\alpha}$ rather than with $\alpha = 1$. Using α different from 1 will modify the model estimates of velocity from those of the purely prognostic run, which will, in turn, modify the values of T, S, and hence ρ_p. Hence the above approach should be viewed as a method of obtaining a reasonable (but not necessarily optimal) estimate of α. Despite this caveat we feel that BLUE provides a practical approach to estimating an appropriate value for the parameter α. In the end, the justification for the approach must come from its performance, and it is the performance of the method we are now ready to evaluate.

In principle, it is possible to go through an iterative procedure by carrying out successive model runs with different values of α in order to determine the optimal value. Such a process would be computationally very expensive and is not used here.

4. Application to the Northwest Atlantic

The ocean circulation model used in this study is the primitive equation z-level model known as CANDIE (the Canadian version of the Dietrich Center for Air Sea Technology (Die CAST)) [*Sheng et al*., 1998]. The original version of CANDIE was developed on the C grid. The results presented in this paper were produced by the A grid version of CANDIE developed by D. G. Wright in consultation with D. Dietrich [*Wright et al*., 2000]. Other model features used in this paper include the fourth-order accurate centered differencing discussed by *Dietrich* [1997] and the multidimensional flux-limited advection scheme discussed by *Thuburn* [1995]. (It should be noted that using the approaches of *Dietrich* [1997] and *Thuburn* [1995] is not necessary for the semiprognostic method to work, but their use does lead to improved numerical accuracy.) The subgrid scale mixing parameterizations include the *Smagorinsky* [1963] scheme for the horizontal eddy viscosity coefficient A_m and the schemes proposed by *Csanady* [1982] and *Large et al*. [1994] for the vertical mixing coefficients K_m and K_h inside and below the surface mixing layer, respectively. The turbulent Prandtl number A_m/A_h is set to 0.1.

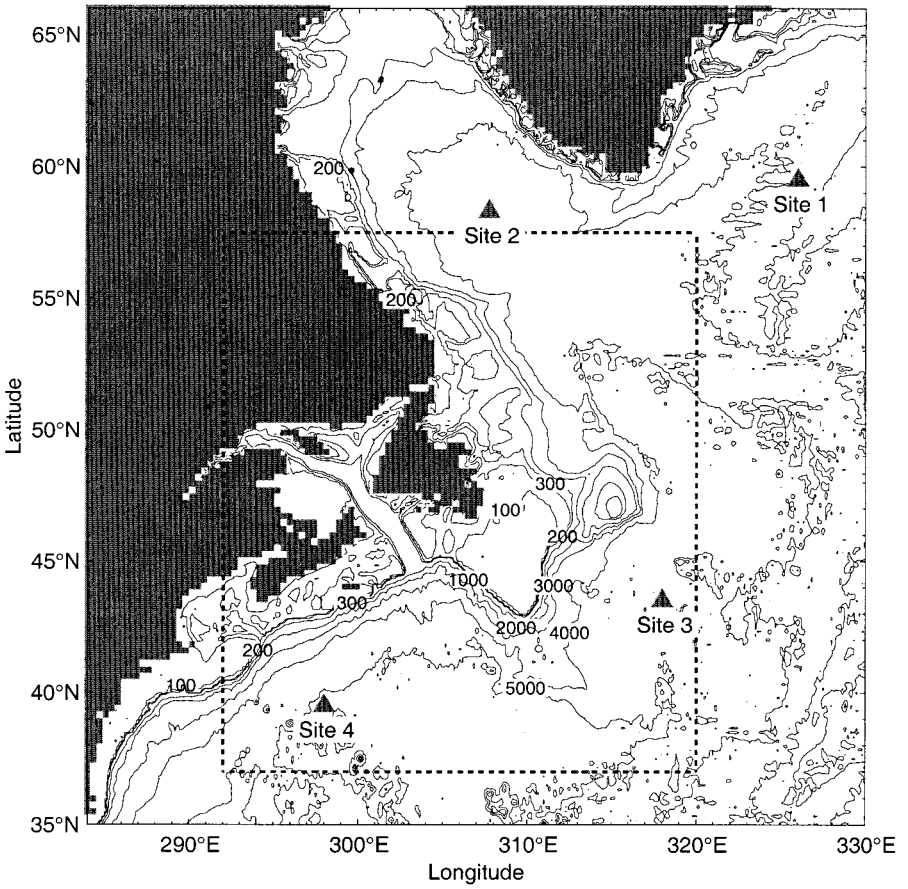

Figure 1. Selected bathymetric features within the model domain of the northwest Atlantic Ocean model. Contours are labeled in units of meters. The area outlined by dashed lines and the locations marked by triangles are chosen to present model results.

The model domain covers the northwest Atlantic Ocean between 284°E and 330°E and between 35°N and 66°N (Figure 1). The model resolution is one third of a degree in longitude, with the grid spacing in latitude chosen so that when measured in kilometers, the grid spacing in the northward and eastward directions remains equal at all latitudes. There are 31 z levels with vertical cell boundaries at depths of 0, 10, 22, 36, 52, 70, 90, 114, 141, 173, 209, 250, 297, 352, 414, 486, 568, 663, 771, 896, 1039, 1203, 1392, 1608, 1857, 2142, 2471, 2847, 3279, 3776, 4346, and 5000 m.

The monthly mean temperature and salinity climatologies used in this study are the set of gridded fields (on a 1/6° by 1/6° grid) recently constructed by *Geshelin et al*. [1999] for the northwest Atlantic. Figures 2 and 3 show the monthly mean temperature climatology interpolated to the model grid at the top z level centered at 5 m and the fifth z level centered at 61 m, respectively. The near-surface waters over the eastern Canadian Shelf are relatively cold and exhibit strong seasonal variability in comparison with the waters offshore from the shelf break. There are also sharp temperature gradients offshore from the continental slopes of the Newfoundland and Scotian Shelves as a result of the interaction between the Labrador Current, the Gulf Stream, and the North Atlantic Current, the three dominant current systems in the region. The sharp temperature gradients are also present at the fifth z level but with much weaker seasonal variability (Figure 3).

The ocean circulation model is initialized with the January climatological temperature and salinity fields and forced by monthly mean Comprehensive Ocean-Atmosphere Data Set (COADS) surface wind stress and heat flux and by flows through the model open boundaries. The net heat flux through the sea surface (Q_{net}) is linearized [*da Silva et al*., 1994] around the climatological sea surface temperature (SST^{clim}) in order to represent the model sea surface temperature ($\text{SST}^{\text{model}}$) feedback on the surface heat fluxes:

$$Q_{\text{net}} \approx Q_{\text{net}}^{\text{clim}} + \beta\,(\text{SST}^{\text{clim}} - \text{SST}^{\text{model}}), \qquad (18)$$

where $Q_{\text{net}}^{\text{clim}}$ is the monthly mean COADS net heat flux out of the ocean interpolated onto the model grid and given by *da Silva et al*. [1994], β is the coupling coefficient defined as $\Delta z_1 \rho_o c_p/\tau_Q$, where Δz_1 is the thickness of the top z level, c_p is the specific heat, and τ_Q is the restoring timescale which is here set to 15 days. The implied value of β is $\sim$35 W m^{-2} K^{-1}, which is comparable to values calculated from observations [e.g., *Haney*, 1971].

The salinity at the 10-m surface layer is restored to monthly mean climatology with a timescale of 15 days. Along the model's open boundaries, temperature and salinity are restored to the monthly mean climatologies, again with the timescale of 15 days. The flow across the open boundaries is taken to be the combination of a baroclinic component determined from density using thermal wind and a barotropic component deter-

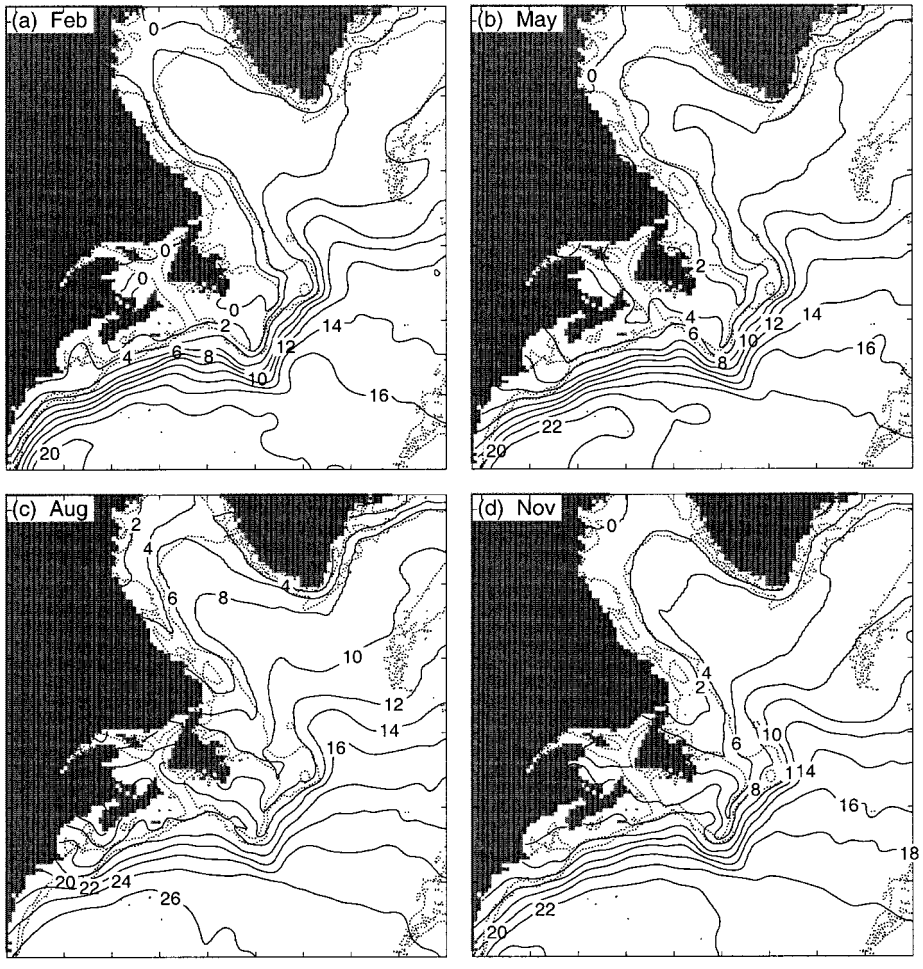

Figure 2. Monthly mean temperature climatology (solid contour lines) at the top z level centered at 5 m in (a) February, (b) May, (c) August, and (d) November. Dotted contour lines represent the 200- and 2000-m isobaths.

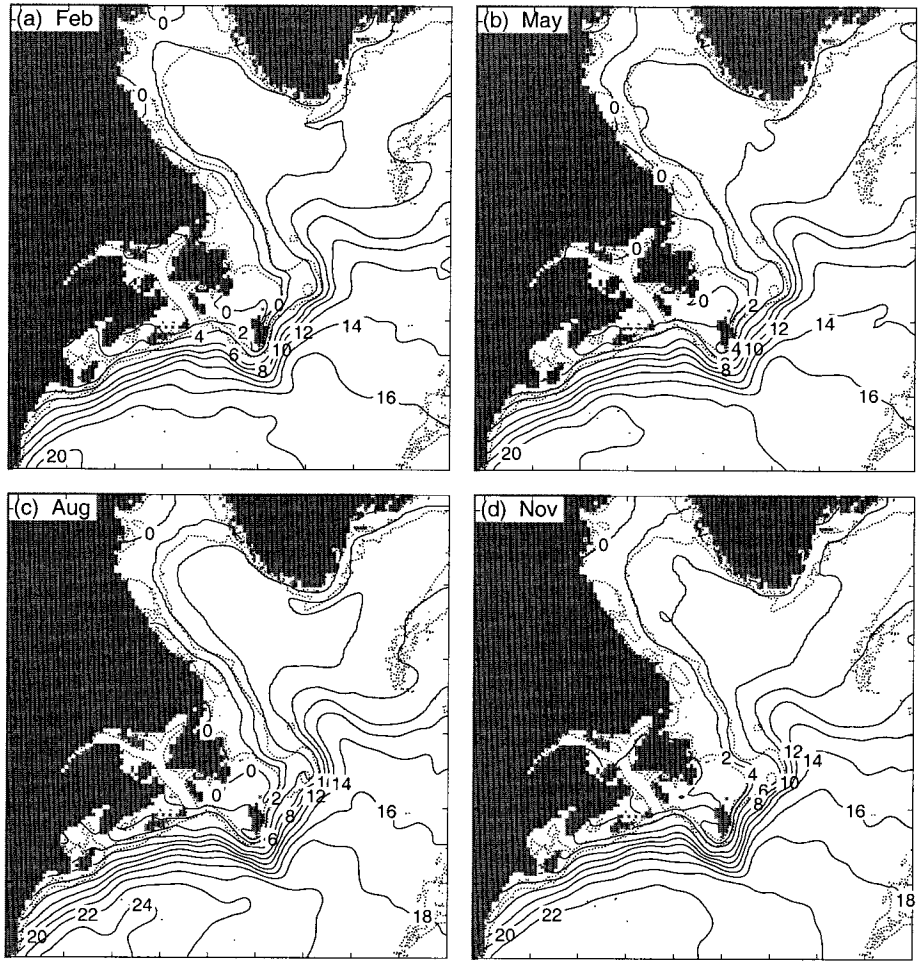

Figure 3. Monthly mean temperature climatology (solid) at the fifth z level centered at 61 m in (a) February, (b) May, (c) August, and (d) November. Dotted contour lines represent the 200- and 2000-m isobaths.

mined from the large-scale diagnostic calculation for the North Atlantic produced by *Greatbatch et al*. [1991].

4.1. Experiment 1: Pure Diagnostic Calculation

First, we ran the ocean circulation model in purely diagnostic mode by setting $\alpha = 0$ in (4). Note that the model temperature and salinity in this experiment are prescribed by the time-varying fields interpolated linearly from the two nearest monthly mean climatological fields. The updated equations for temperature and salinity defined in (7) and (8) and the corresponding sea surface and lateral boundary conditions are not needed in the diagnostic calculation.

Figure 4 presents the annual mean transport stream functions for the second year of the diagnostic run. The annual mean transport for the third and fourth years of the simulation are identical to the second-year simulation, as expected. The diagnostic calculation reproduces the expected mean transport circulation in the northwest Atlantic Ocean reasonably well, including the western Greenland and Labrador Currents, the Gulf Stream and North Atlantic Current in the deep waters off the Newfoundland and Scotian Shelves, and the counterclockwise recirculation between the Scotian Shelf and the Gulf Stream. The maximum annual mean transports produced by the diagnostic calculation are ~50 sverdrup (Sv) for the Labrador Current system east of Labrador, 90 Sv for the Gulf Stream, and 10 Sv for the recirculation in the slope region off the Scotian Shelf, comparable to the results of previous diagnostic modeling studies [e.g., *Mellor et al*., 1982; *Greatbatch et al*., 1991].

To assess the model performance, we compared the monthly mean currents produced by the diagnostic run during the second year of the simulation with monthly mean current meter observations made in the region. The data were extracted from a database compiled at the Bedford Institute of Oceanography. Note that only observations with a recorded length >15 days in any one month were used. Furthermore, horizontal and vertical averaging was carried out if more than one observational record was available in a control volume of the model grid. In spite of the above averaging it is clear that these observational current estimates will include significant contributions from eddies, which we do not expect to correlate with model results. Nevertheless, they provide a useful benchmark with which to make comparisons. Figure 5 shows the horizontal locations of the current meter observations after the averaging. It can be seen that most of the observations were made over the Canadian Shelf waters, with very few observations offshore from the shelf.

Figure 6 compares the model-computed and observed monthly mean currents at the fifth z level centered at 61 m (from 52 to 70 m) over the area outlined by a dashed box in Figure 1. The diagnostic calculation produces a narrow southeastward jet along the shelf breaks of the Labrador and Newfoundland Shelves, known as the offshore branch of the Labrador Current, with a maximum speed of ~40 cm s^{-1}, which is consistent with observations [e.g., *Lazier and Wright*, 1993]. The other two branches of the Labrador Current, the inshore branch in the coastal region and the deep branch beyond the shelf break, are relatively weak at this particular z level. On reaching the northern flank of the Grand Banks, the offshore branch of the Labrador Current splits into three parts: a coastal branch that flows through the Avalon Channel, a middle branch that flows through Flemish Pass to the south, and an eastern branch that passes around the seaward flank of Flemish Cap. The middle branch and part of the eastern branch merge over the eastern flank of the Grand Banks, forming a narrow equatorward jet along the shelf breaks of the Grand Bank and the Scotian Shelf, with typical speeds of ~30 cm s^{-1}. The existence of this shelf break jet has been confirmed by previous measurements [e.g., *Webster*, 1969; *Smith and Petrie*, 1982; *Loder et al*., 1988]. The diagnostic calculation also produces reasonable estimates of the general flow patterns of the Gulf Stream and North Atlantic Current offshore from the continental slopes of the Grand Banks and the Scotian Shelf.

It can be seen from Figure 6 that most of the current meter observations at this z level were made on the Scotian Shelf and in the Gulf of St. Lawrence. The diagnostic results in these regions agree reasonably well with the observations, particularly the southwestward narrow jet along the Scotian Shelf break.

Figure 7 shows scatterplots of model-computed and observed monthly mean currents in the full model domain at all z levels <20 m (the nominal depth of the surface mixed layer). We measured the misfit between the observations and the model using the value of γ^2 defined as

$$\gamma^2 = \frac{\sum[|\vec{U}|_{\text{obs}} - |\vec{U}|_{\text{pred}}]^2}{\sum|\vec{U}|^2_{\text{obs}}}, \tag{19}$$

where $|\vec{U}|_{\text{pred}}$ and $|\vec{U}|_{\text{obs}}$ are the speeds of model-computed and observed currents, respectively. For the data shown in Figure 7, γ_d^2 is ~0.6, and the linear correlation between $|\vec{U}|_{\text{pred}}$ and $|\vec{U}|_{\text{obs}}$ with the 90% confidence level is 0.38 ± 0.08.

4.2. Experiment 2: Purely Prognostic Calculation

Next, we ran the ocean circulation model in pure prognostic mode by setting $\alpha = 1$ in (4). Figure 8 shows annual mean volume transport stream functions averaged over each of the 4 years of the model simulation. The prognostic results in the first year compare well with the diagnostic model, with many well-known large-scale circulation features being reproduced (compare Figures 4 and 8a). The maximum transports produced by the prognostic calculation in the first year are slightly less than 50 Sv for the Labrador Current, ~80 Sv for the Gulf Stream, and 10 Sv for the recirculation in the slope region between the Scotian Shelf and Gulf Stream and are comparable to transports found in the diagnostic calculation.

The prognostic model performance, however, deteriorates significantly after the first year, particularly in simulating the Gulf Stream and the North Atlantic Current. Figure 8b shows that the North Atlantic Current produced by the prognostic calculation is much weaker, and the Gulf Stream is less coherent in the second year of the simulation than in the first. By the fourth year the maximum transport of the Labrador Current is reduced to ~30 Sv, and the main path of the Gulf Stream is shifted southward to near the model's open southern boundary (Figure 8d). Since the horizontal flow is close to being in geostrophic balance, there is a strong coupling between these errors in the model-computed velocity field and errors in the model-computed density field. Figure 9 shows the model-computed monthly mean temperature at the fifth z level (61 m) during the second year. In comparison with the climatological temperature at the same z level shown in Figure 3, the pure prognostic calculation fails to maintain the strong temperature fronts in the deep waters off the Newfoundland and Scotian Shelves.

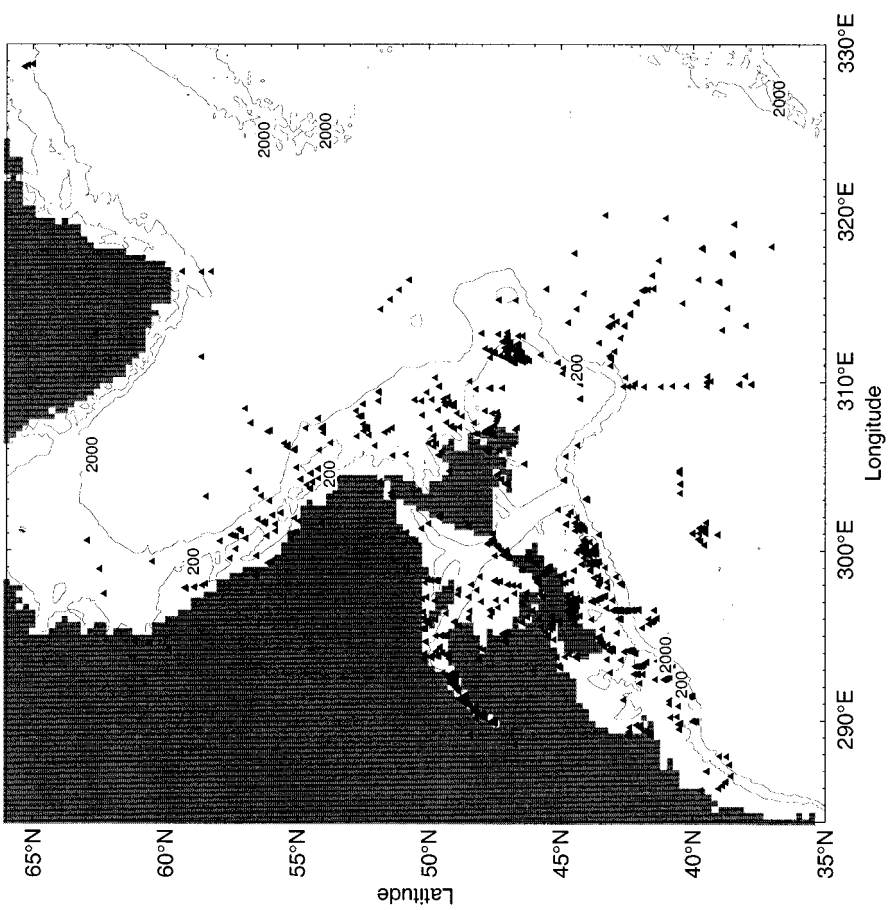

Figure 5. Horizontal positions of current meter observations with recorded lengths >15 days in any one month. The data are extracted from a database compiled at the Bedford Institute of Oceanography. The thin contour lines represent the 200- and 2000-m isobaths.

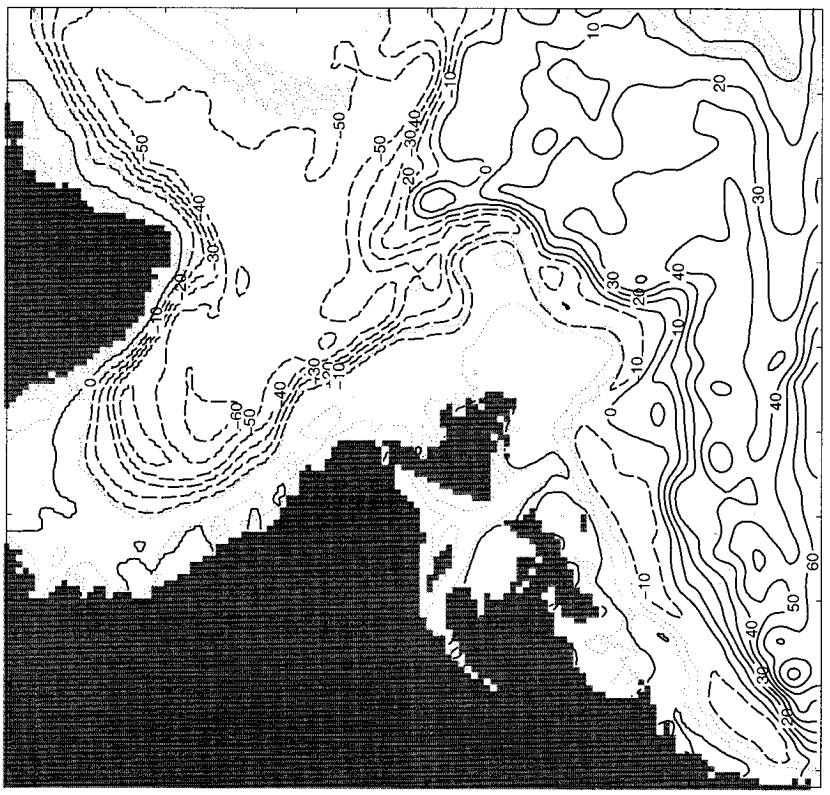

Figure 4. Annual mean volume transport stream function (solid and dashed lines) for the second year of the diagnostic run. Contours (solid and dashed lines) are labeled in units of sverdrup ($=10^6$ m^3 s^{-1}). Dotted contour lines represent the 200- and 2000-m isobaths.

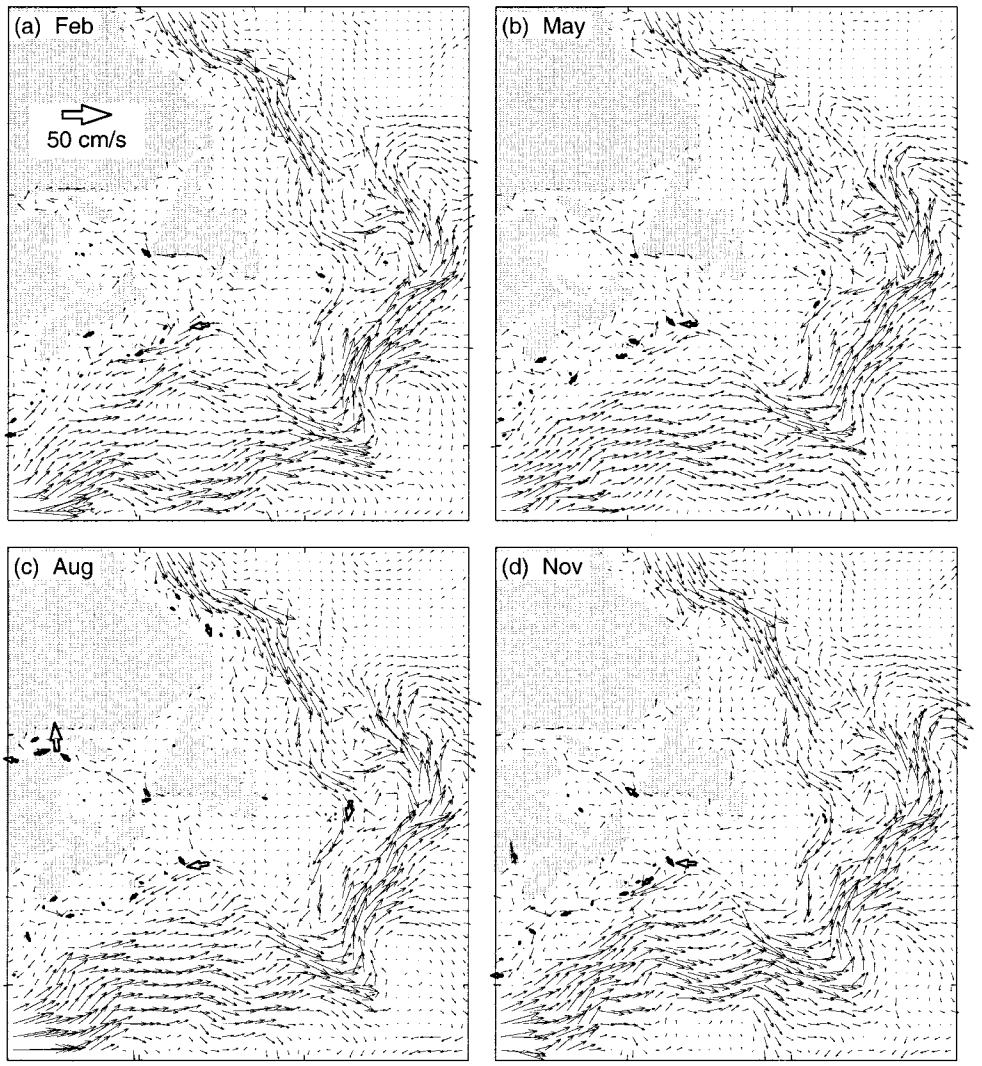

Figure 6. Monthly mean currents at the fifth z level centered at 61 m in (a) February, (b) May, (c) August, and (d) November, averaged from the second year of the diagnostic run. The velocity vectors are plotted at every second model grid point. The open arrows show the current meter observations for comparison with the model. Dotted contour lines represent 200- and 2000-m isobaths.

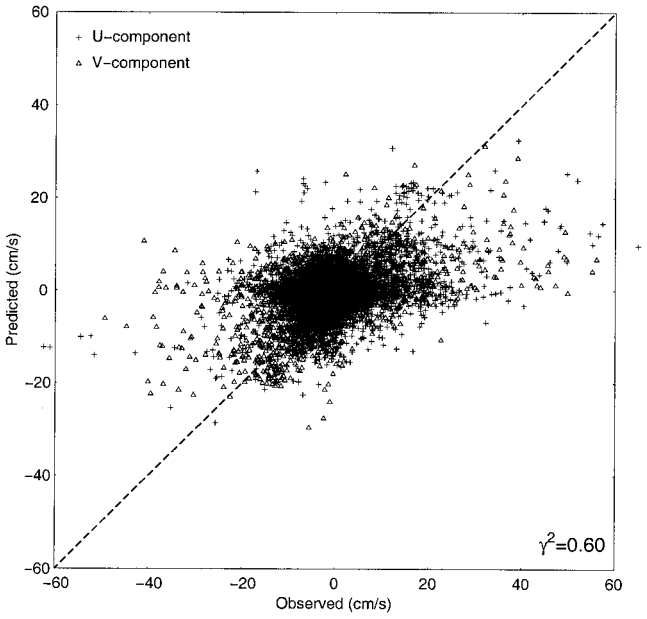

The reasons for the deteriorating performance of the pure prognostic calculation are not clear, although contributing factors could include lack of resolution, inadequate parameterization of unresolved processes, the formulation and specification of the open boundary conditions, or inadequate surface boundary conditions (e.g., the model does not include synoptic variability in its surface forcing), all of which are common problems with models.

Figure 10 presents time-depth distributions of monthly mean temperature produced by the prognostic calculation at sites 2 and 3 (Figure 1). Figure 10 illustrates the gradual establishment of upper ocean stratification in spring and summer and the relatively rapid establishment of cold, weakly stratified waters in fall and winter. This is consistent with the fact that

Figure 7. (opposite) Scatterplot of observed and model-computed monthly mean currents in the northwest Atlantic. The model-computed currents are from the second year of the pure diagnostic run.

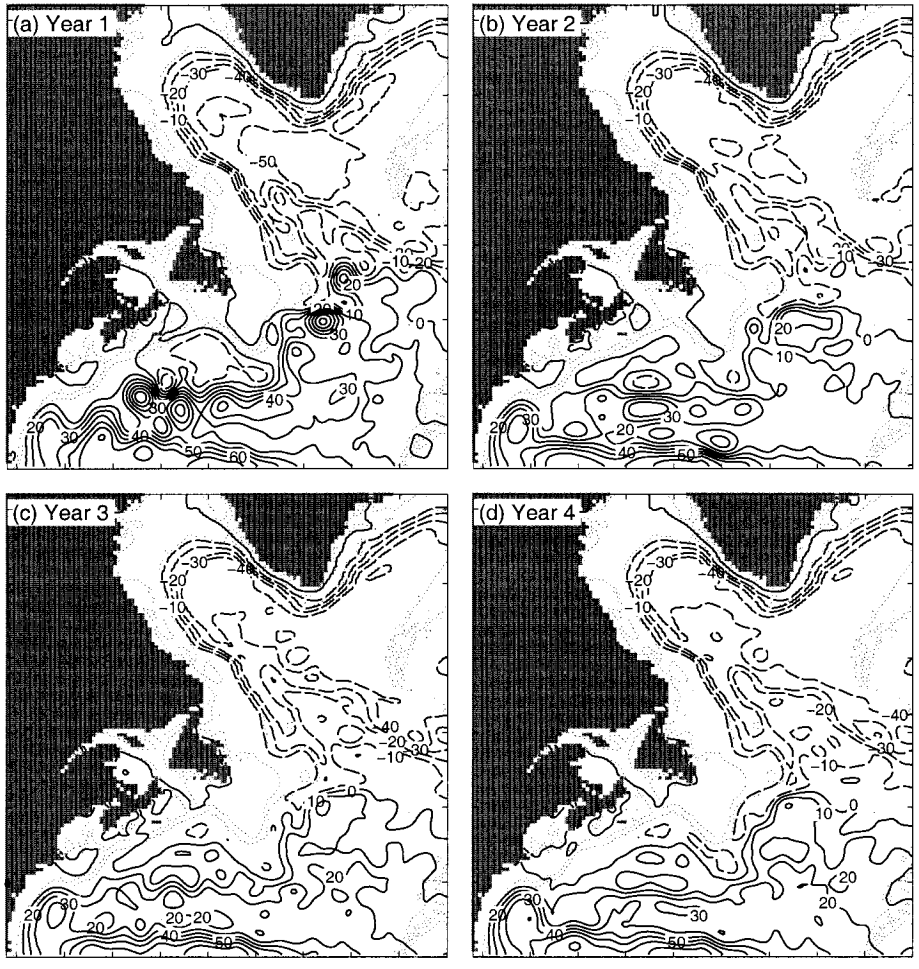

Figure 8. Annual mean volume transport stream function (solid and dashed lines) for each of the 4 years of the prognostic run: (a) year 1, (b) year 2, (c) year 3, and (d) year 4. Contours are labeled in units of sverdrup ($=10^6$ m^3 s^{-1}). Dotted contour lines represent the 200- and 2000-m isobaths.

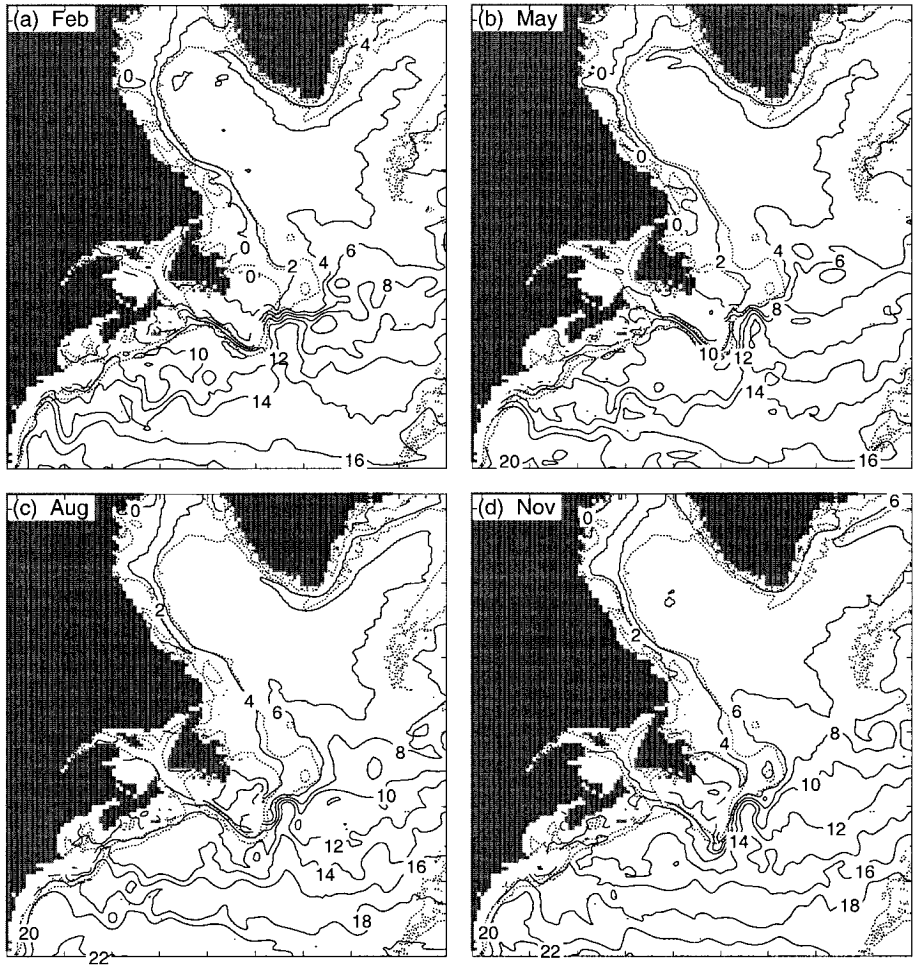

Figure 9. Monthly mean temperature (solid) at the fifth z level centered at 61 m in (a) February, (b) May, (c) August, and (d) November, averaged from the second year of the prognostic run. Dotted contour lines represent the 200- and 2000-m isobaths.

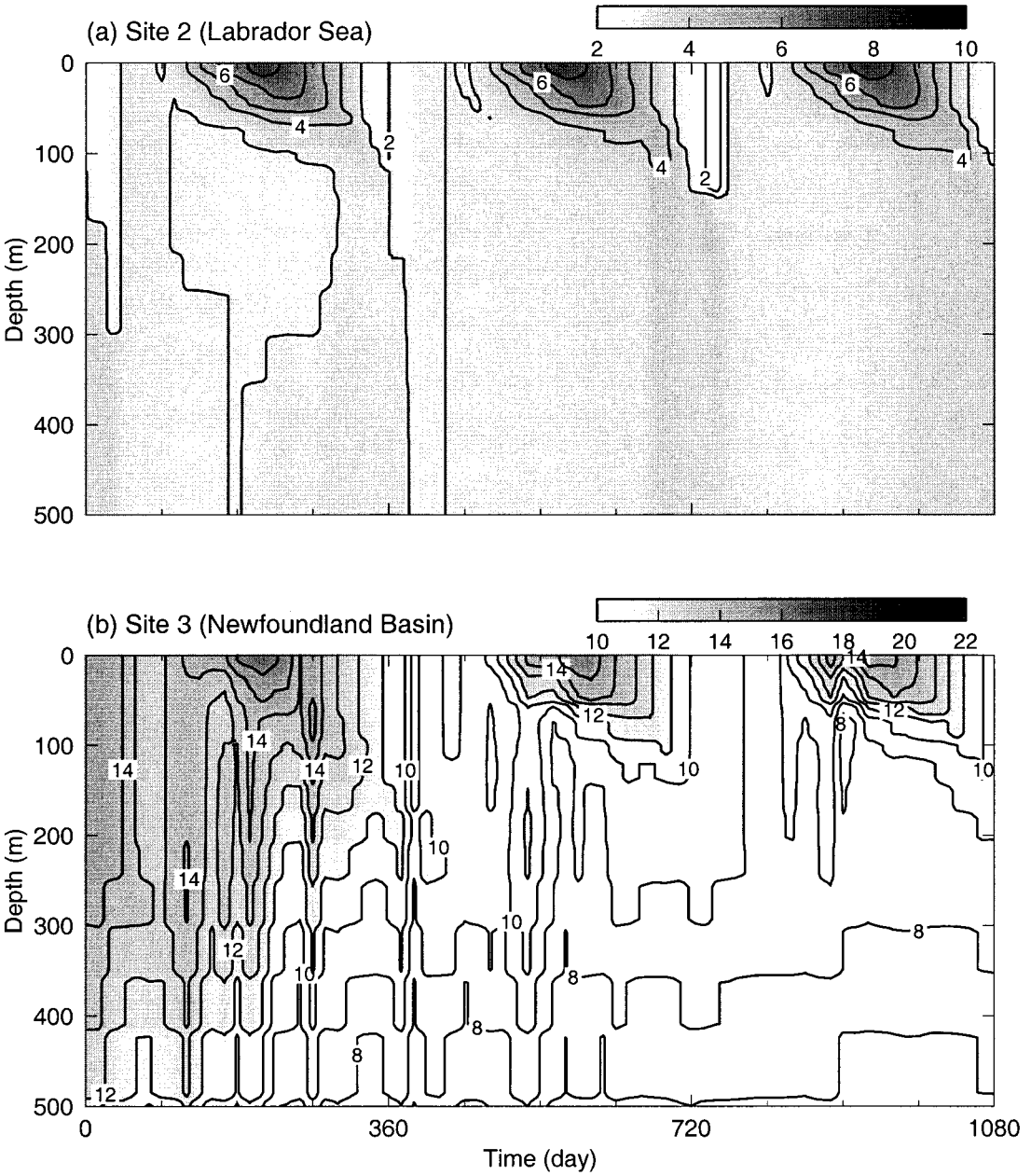

Figure 10. Time-depth distributions of monthly mean temperature from the first 3 years of the prognostic run at the sites located in (a) the Labrador Sea and (b) the Newfoundland Basin shown in Figure 1. Only the top 500 m is shown.

the upper ocean in this region has relatively weak vertical mixing in spring and summer, due to weak winds and the stable stratification associated with surface heating, but relatively strong mixing in fall and winter, associated with stronger winds and surface cooling. Figure 10 also shows that the pure prognostic calculation reasonably reproduces the expected seasonal cycle of upper water temperature at site 2 but does less well at site 3. The subsurface water temperature at site 3 produced by the prognostic run is ~4°C colder in the second and third year in comparison with the first year of the simulation.

Figure 11 shows the comparison of model-computed and climatological monthly mean temperatures at five z levels in the upper water column at the four selected sites. The prognostic calculation does reasonably well at sites 1 and 2 but does poorly at the other two sites, particularly at site 3, where the model-computed temperature is too low in comparison with climatology. An examination of Figures 8 and 9 indicates that the poor model performance at sites 3 and 4 is associated with the collapse of the near-surface temperature fronts in the deep waters off the continental slopes of the Grand Banks and the Scotian Shelf.

Through geostrophy the collapse of the temperature (and therefore density) fronts in the deep waters leads to the model-computed currents produced by the prognostic run straying farther away from the observations than was the case for the diagnostic calculation. Figure 12 shows the model-computed and observed monthly mean currents at the fifth z level. In comparison with the diagnostic results shown in Figure 6, the

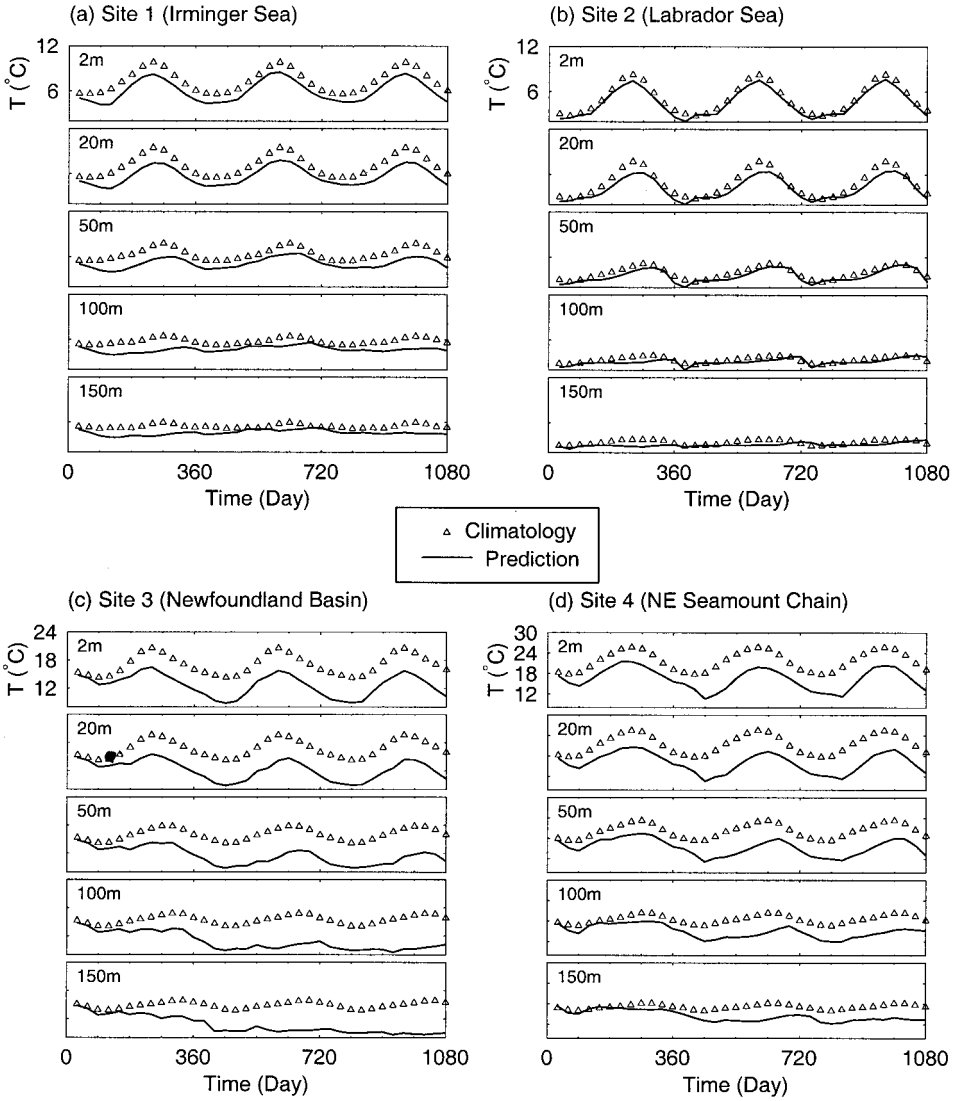

Figure 11. Comparison of monthly mean observed and model-computed temperature at the four sites shown in Figure 1. Five z levels in the upper 150 m are shown. The model-computed temperatures are from the pure prognostic run.

prognostic calculation in the second year significantly underestimates the general circulation in the region, particularly the Gulf Stream and North Atlantic Current. Furthermore, the prognostic run also did poorly in reproducing the narrow jet along the shelf break off the Grand Banks and the Scotian Shelf where the model currents are generally in the opposite direction of the observations.

Figure 13 shows a scatterplot of observed monthly mean currents and those obtained from the second year of the prognostic run. In comparison with the diagnostic results shown in Figure 7, the prognostic results shown in Figure 13 are much more scattered, with a γ_p^2 value of >0.7 and a linear correlation of 0.31 ± 0.08, indicating the reduced skill of the prognostic calculation in comparison with the diagnostic calculation. Note that the γ^2 value for the first half year of the prognostic calculation is smaller than that for the diagnostic run, indicating that the prognostic calculation has better skill in a short model simulation, which is consistent with the finding of *Ezer and Mellor* [1994]. Finally, we note that the pure prognostic calculation has sufficient resolution and is sufficiently inviscid to exhibit mesoscale variability, a topic we return to in section 5.

4.3. Experiment 3: Semiprognostic Calculation

The first step in applying the "semiprognostic" method is to estimate the linear combination coefficient from the error variances σ_p^2 and σ_d^2 according to (17). In this paper we approximate σ^2 by γ^2 defined in (19), with σ_p^2 being γ^2 computed for the purely prognostic run and σ_d^2 being γ^2 for the diagnostic run. On the basis of an average over 1 year we estimated the value of α to be ~ 0.45. We note, however, that if results from only the first half year of the prognostic run are used in determining γ_p^2, then the estimate of α would be slightly greater than 0.5, since the pure prognostic run does slightly better than the pure diagnostic run over this time interval. We also note that the value of γ_p should actually be based on the results from the semiprognostic calculation since this is the density ρ_p that is used in (4). In anticipation of the fact that the semiprognostic results will be more accurate than the

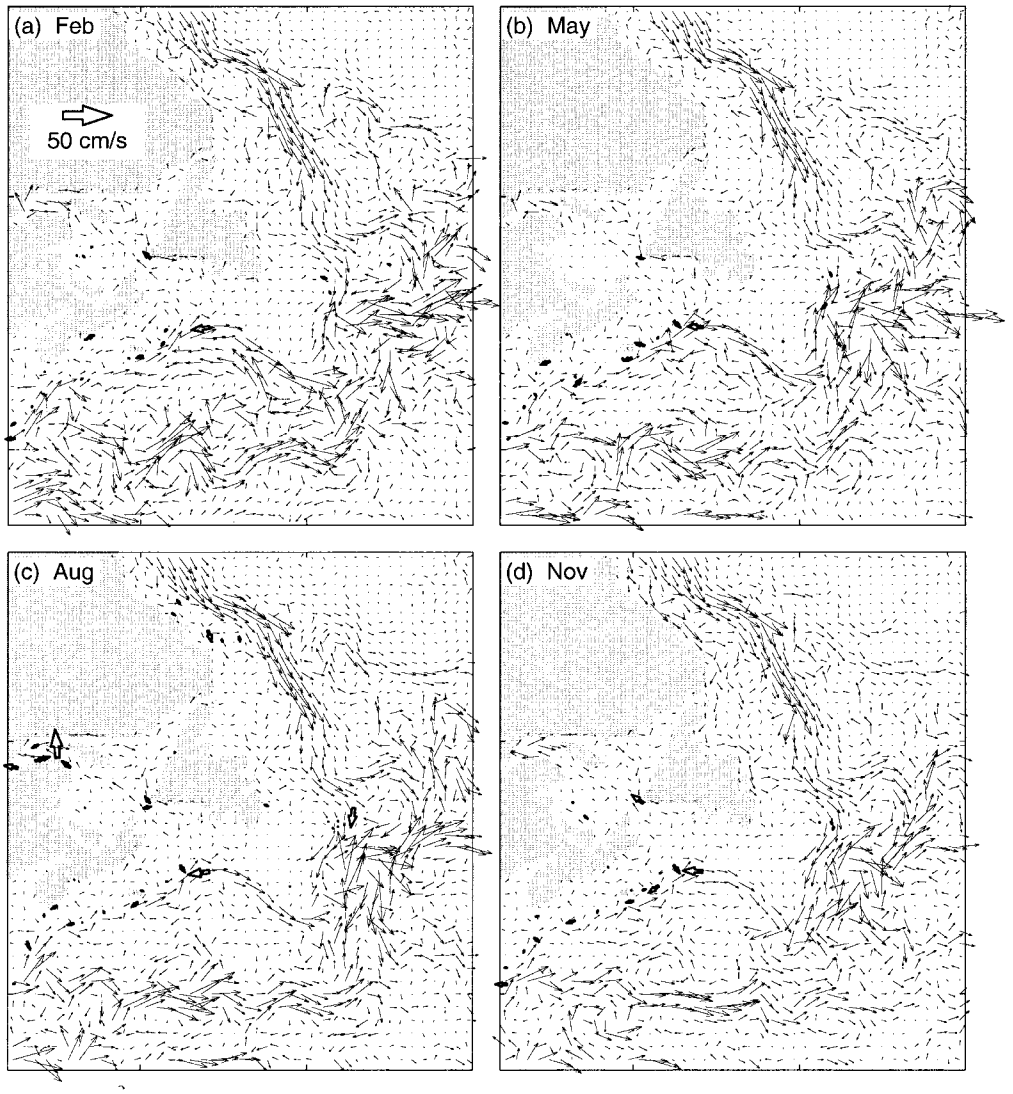

Figure 12. Monthly mean currents at the fifth z level centered at 61 m in (a) February, (b) May, (c) August, and (d) November from the second year of the prognostic run. The velocity vectors are plotted at every second model grid point. The open arrows show the current meter observations for comparison with the model. Dotted contour lines represent the 200- and 2000-m isobaths.

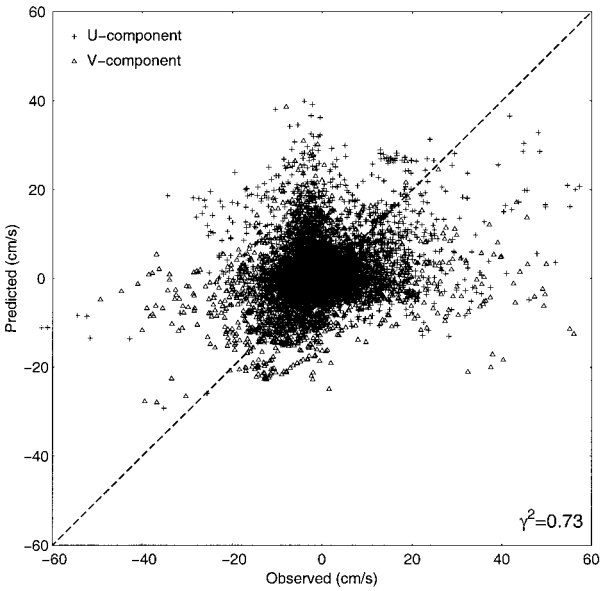

Figure 13. (opposite) Scatterplot of observed and model-computed monthly mean currents in the northwest Atlantic. The model-computed currents are from the second year of the pure prognostic run.

purely prognostic results, we use $\alpha = 0.5$ in the semiprognostic run. We return to this point below, although there is actually very little difference in the model results for α between 0.4 and 0.6. Finally, we note that since most current meter observations were made over the eastern Canadian Shelf region, the optimal value of α based on γ^2 is biased to the circulation in the shelf regions rather than to that in the deep waters.

Figure 14 shows the annual mean transport stream functions from the semiprognostic run averaged for each of the 4 years of the model simulation. The semiprognostic run performs much better than the pure prognostic run, particularly in the third and fourth years. The maximum annual mean transport in the second year produced by the semi-

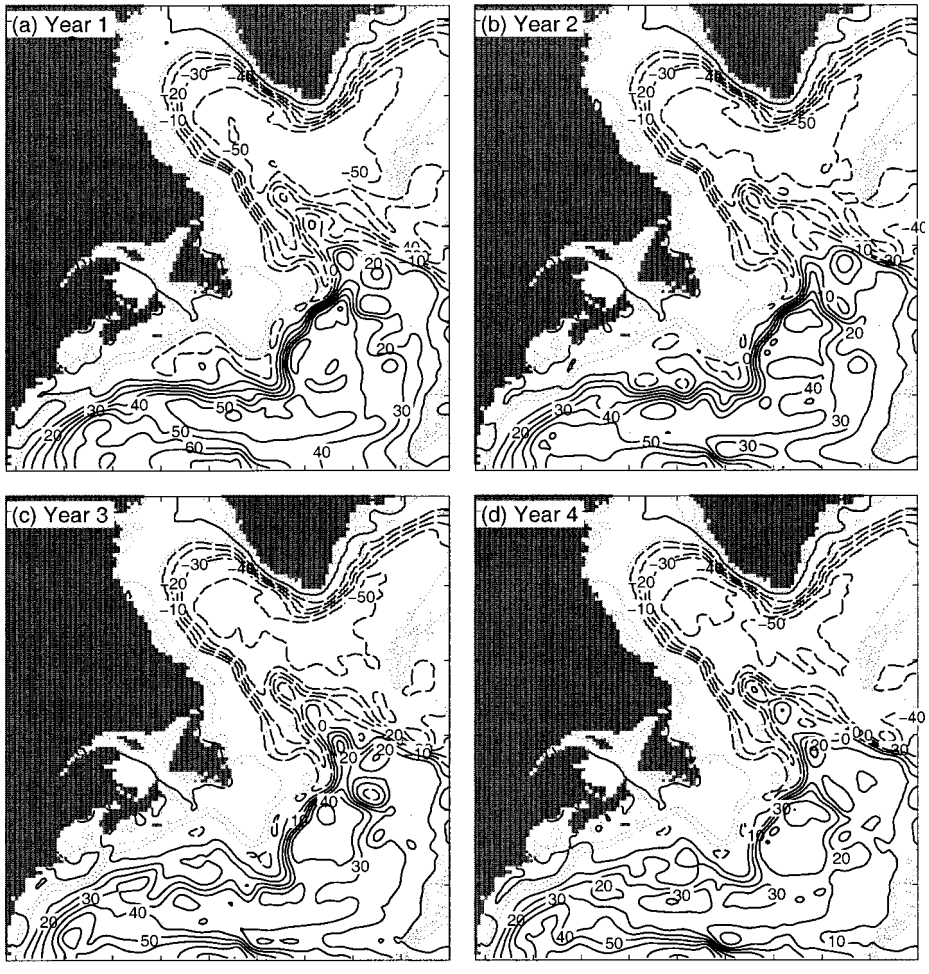

Figure 14. Annual mean volume transport stream function (solid and dashed lines) for each of the 4 years of the semiprognostic run. Contours are labeled in units of sverdrup ($=10^6$ m^3 s^{-1}). Dotted contour lines represent the 200- and 2000-m isobaths.

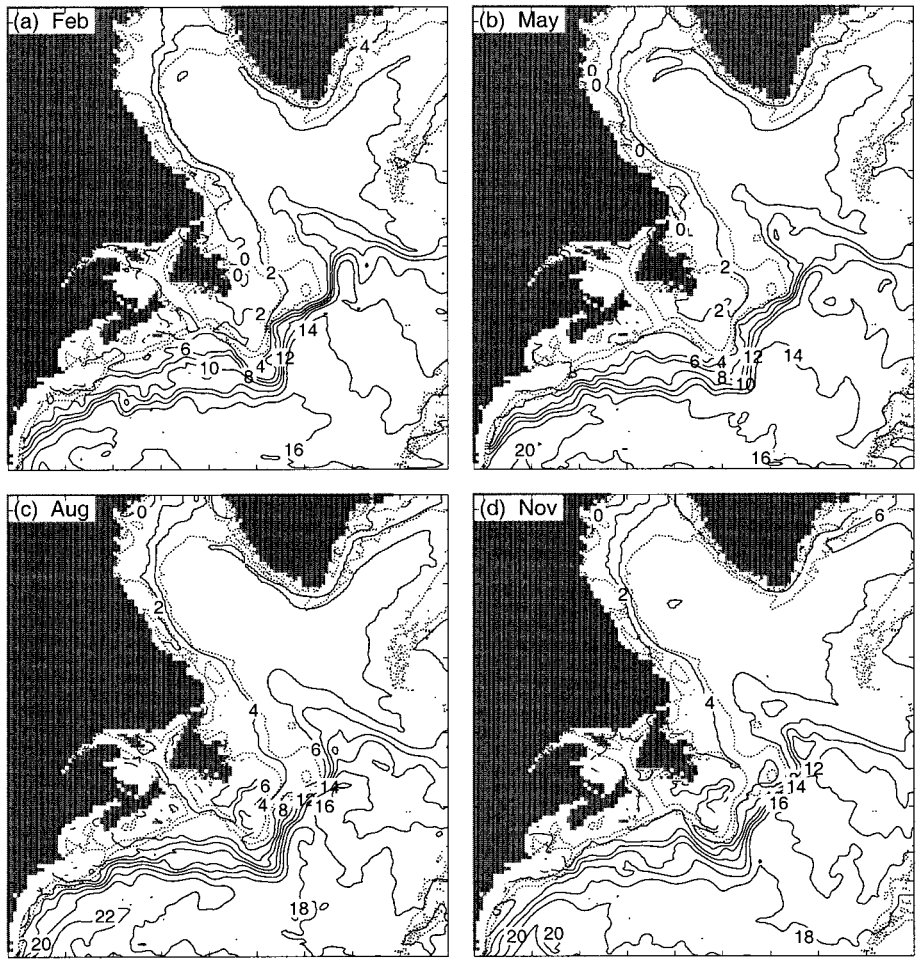

Figure 15. Monthly mean temperature (solid line) at the fifth z level centered at 61 m in (a) February, (b) May, (c) August, and (d) November from the second year of the semiprognostic run. Dotted contour lines represent the 200- and 2000-m isobaths.

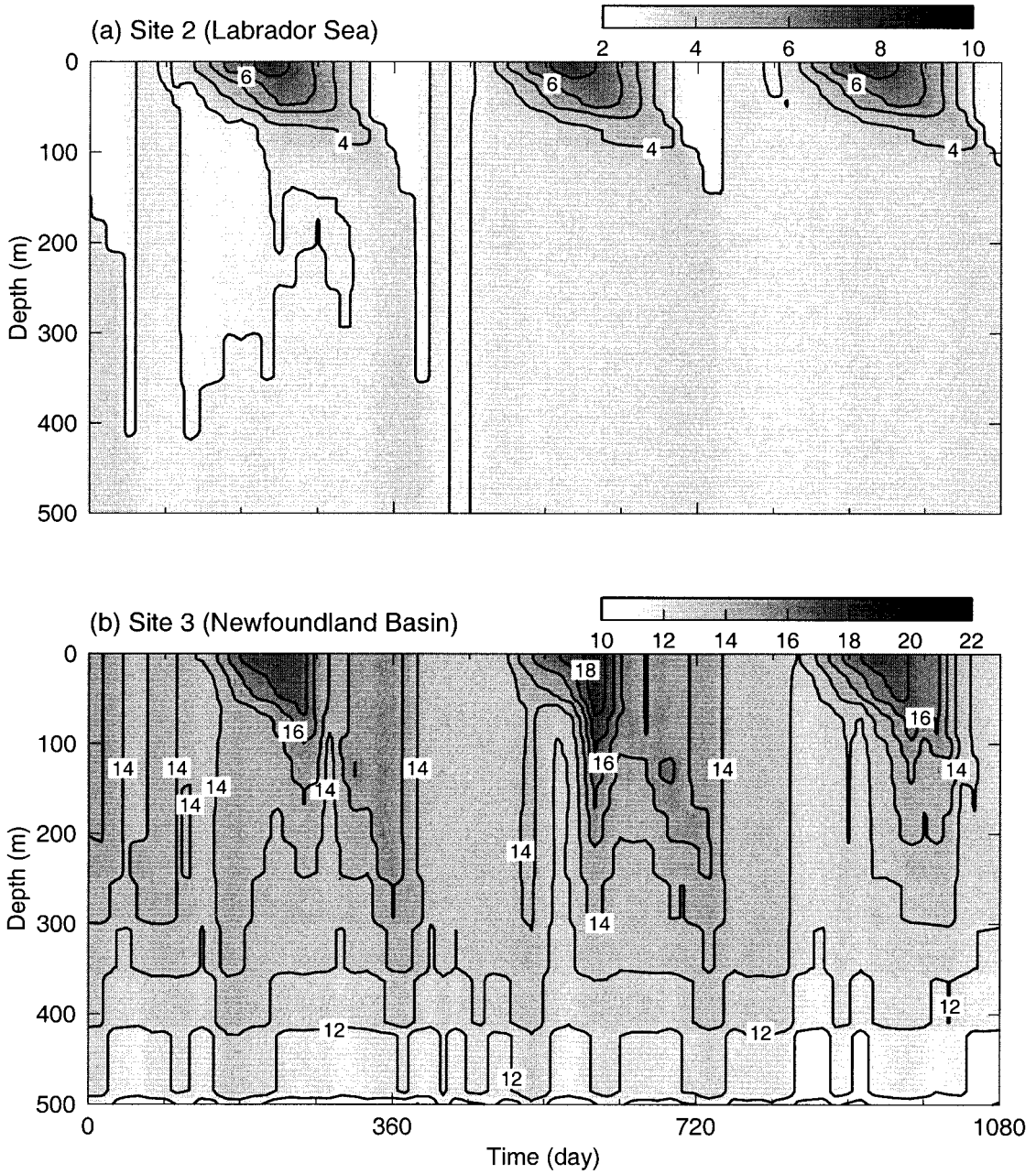

Figure 16. Time-depth distributions of monthly mean temperature from the first 3 years of the semiprognostic run at the two sites in (a) the Labrador Sea and (b) the Newfoundland Basin shown in Figure 1. Only the top 500 m is shown.

prognostic run is ~50 Sv for the Labrador Current system, 90 Sv for the Gulf Stream, and 10 Sv for the recirculation in the slope region between the Scotian Shelf and the Gulf Stream (Figure 14b), which are consistent with the results produced by the diagnostic run. Note that the semiprognostic results are expected to compare better with the diagnostic results than the pure prognostic results. However, the agreement between the semiprognostic and diagnostic results is better than what would be obtained by simply taking a weighted mean of the diagnostic and prognostic results. The additional improvement reflects the substantially reduced drift of the tracer fields experienced in the semiprognostic run.

As noted in section 2, the temperature and salinity equations are unconstrained in the semiprognostic approach. It follows that temperature and salinity are particularly useful in assessing the model performance. Figure 15 shows the monthly mean temperature fields at the fifth z level averaged over the second year of the semiprognostic simulation. In comparison with the pure prognostic results shown in Figure 9, the semiprognostic method has significantly improved the model performance in maintaining the temperature (and density) fronts in the deep waters. Furthermore, in comparison with the climatology shown in Figure 3, the semiprognostic method has also significantly improved the temperature fronts in the deep waters.

Figure 16 demonstrates that the semiprognostic calculation reasonably reproduces the seasonal cycles of upper ocean temperature and vertical mixing processes at the two sites. In

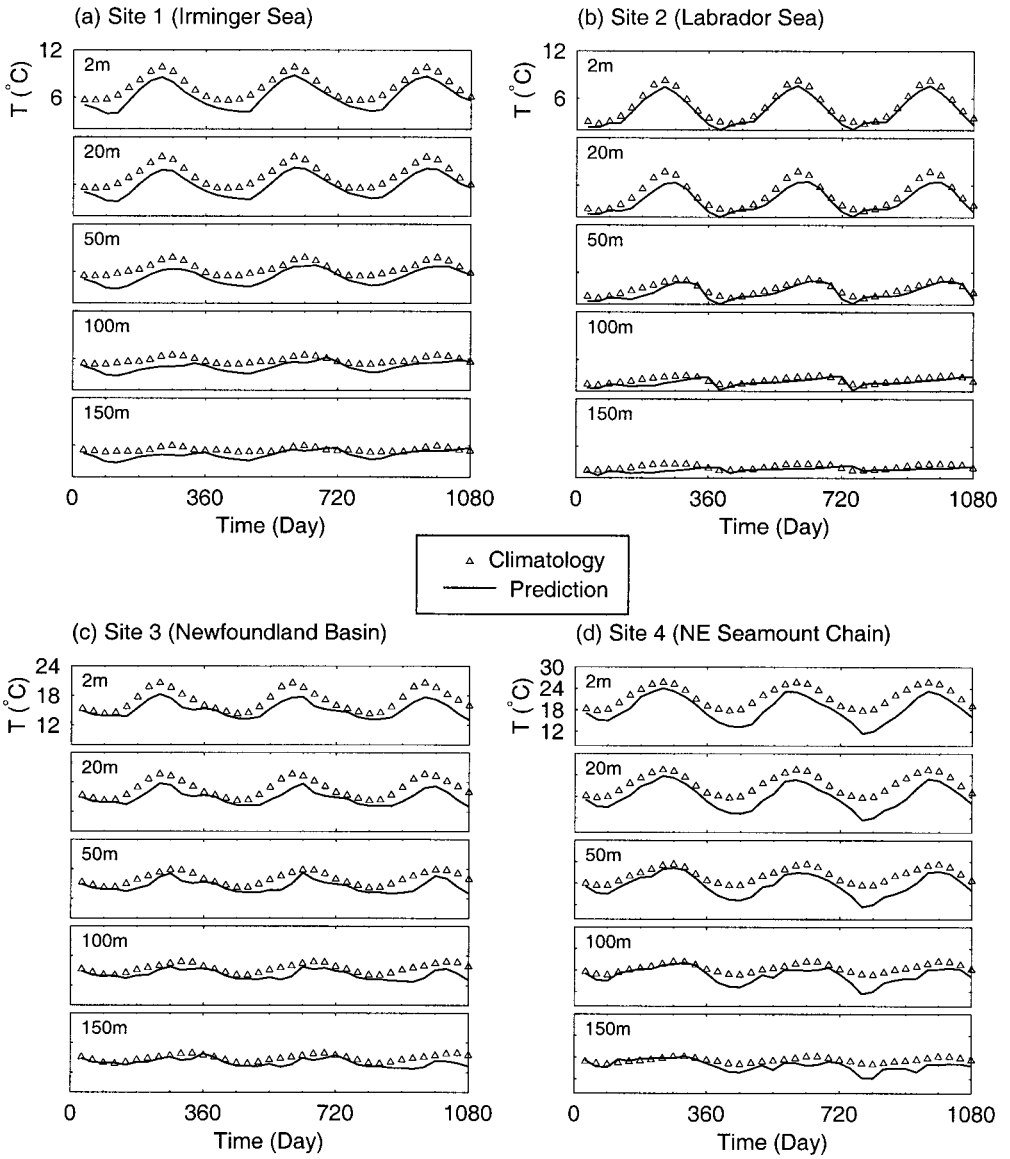

Figure 17. Comparison of observed and model-computed monthly mean temperatures at the four sites shown in Figure 1. Five z levels in the upper 150 m are shown. The model-computed temperatures are from the semiprognostic run.

comparison with the pure prognostic results shown in Figure 10, the semiprognostic method significantly improves the model results at site 3. Figure 17 also shows that by using the semiprognostic method, good agreement is achieved between the climatology and model-computed temperatures at all four sites.

It is relatively easy to understand why the semiprognostic calculation is better than the pure prognostic calculation in simulating the tracer fields in the northwest Atlantic Ocean. It is readily seen that advection processes play a very important role in the temperature and salinity fields in the northwest Atlantic Ocean. Since the semiprognostic method significantly reduces the drifts of the model velocity fields away from the climatology, it simulates well the tracer advection processes, leading to a better performance in reproducing the temperature and salinity fields in the region in comparison with the pure diagnostic calculation.

Figure 18 illustrates the ability of the semiprognostic approach to reproduce the monthly mean circulation in the region. The large-scale features of the currents computed using the semiprognostic method are very similar to the diagnostic results, as expected. The γ^2 value in the semiprognostic run is ~0.55 (Figure 19), which is the smallest among the three different experiments. The linear correlation between $|\vec{U}|_{\text{pred}}$ and $|\vec{U}|_{\text{obs}}$ with the 90% confidence level in this run is 0.45 ± 0.07, which is the highest. Therefore the semiprognostic calculation also is the best, although marginally, in simulating the ocean currents in comparison with the pure diagnostic and prognostic runs. We note that this result suggests that the value of α could have been chosen slightly greater than 0.5, but experiments with different values of α show that the effect of small variations around the value of 0.5 is rather minor.

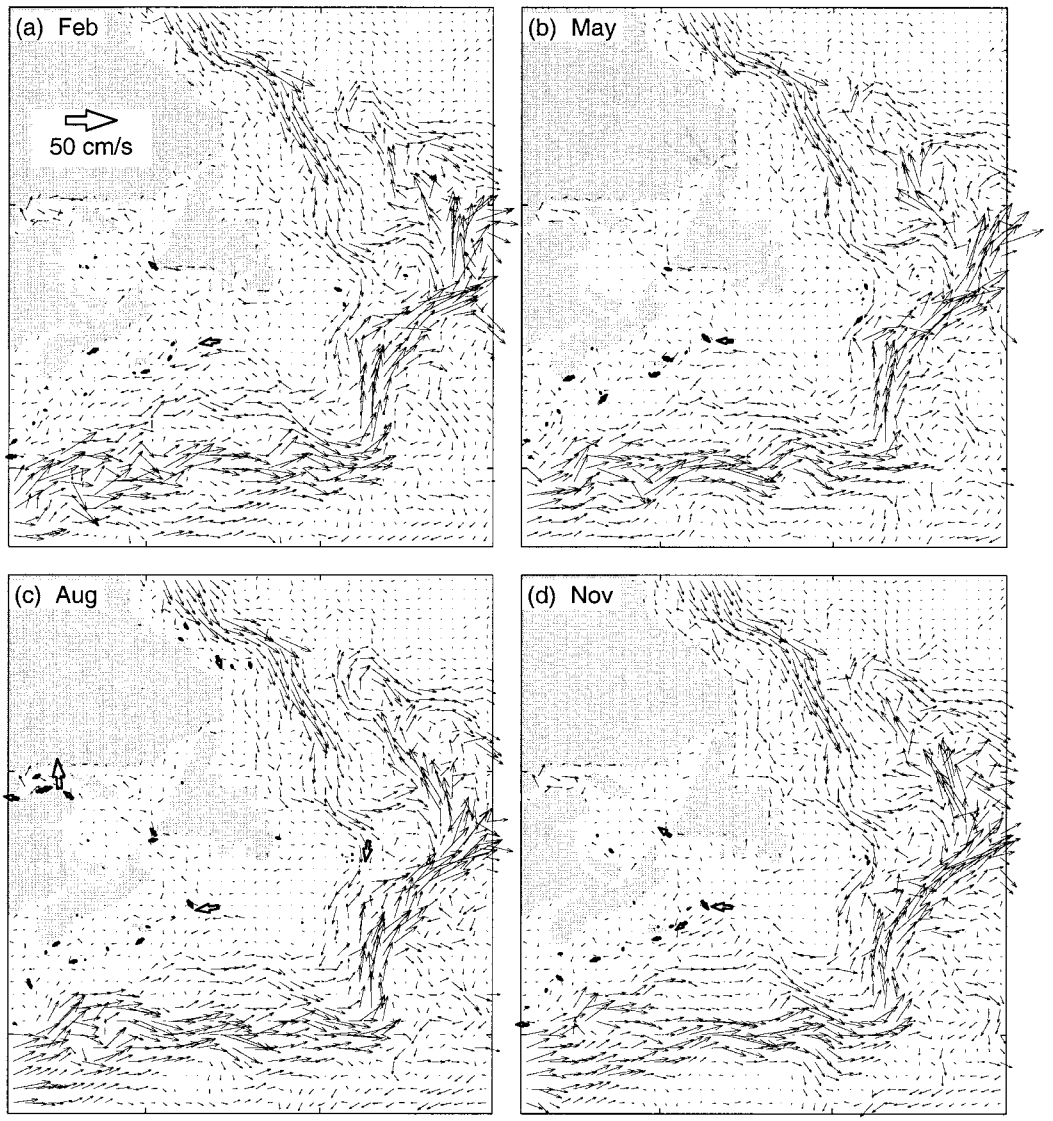

Figure 18. Monthly mean currents at the fifth z level centered at 61 m in (a) February, (b) May, (c) August, and (d) November from the second year of the semiprognostic run. The velocity vectors are plotted at every second model grid point. The open arrows show the current meter observations for comparison with the model. Dotted contour lines represent the 200- and 2000-m isobaths, respectively.

5. Summary

Numerical ocean models with prognostic dynamics are increasingly used to simulate three-dimensional ocean currents, tracer distributions, and their variability. It is often found, however, that prognostic calculations gradually drift away from climatology. In this paper we propose a straightforward method to improve the utility of primitive equation ocean circulation models. The essence of the method is to use observed temperature and salinity data (in our case, climatological data) to add forcing terms to the horizontal momentum equations in the model, while leaving the model temperature and salinity equations fully prognostic and unconstrained. This is accomplished by replacing the density term in the hydrostatic equation by a linear combination of model-computed and climatological density. Assuming the linear combination coefficient to be invariant in time and space, we suggest that the statistical approach known as the best linear unbiased estimator can be used to estimate an appropriate value of the coefficient, while noting that the method is strictly only valid for linear systems (our model uses nonlinear equations to update momentum, temperature, and salinity). The new method has the advantage over the robust diagnostic method suggested by *Sarmiento and Bryan* [1982] in that it does not use artificial internal sources and sinks of heat and salt to push the model results toward climatology. For this reason we refer to the new method as being semiprognostic.

We applied the semiprognostic method to the northwest Atlantic and compared the model results with those produced by pure diagnostic and pure prognostic runs. The pure diagnostic run for the northwest Atlantic reasonably reproduces the large-scale transport stream functions and three-dimensional currents estimated from previous diagnostic modeling studies and from current meter observa-

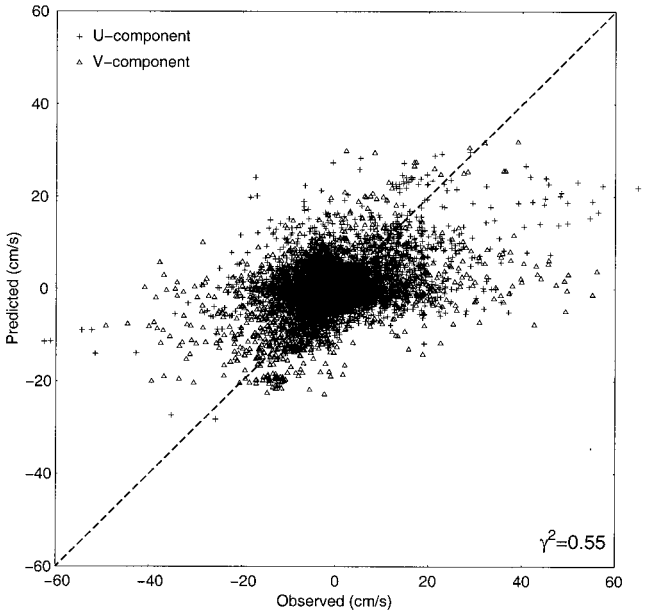

Figure 19. Scatterplot of observed and model-computed monthly mean currents in the northwest Atlantic. The model-computed currents are from the second year of the semiprognostic model run.

tions. The main drawback of a diagnostic run is, of course, that the temperature and salinity fields are specified. In contrast, a pure prognostic calculation includes more complete physics since temperature and salinity are computed prognostically as part of the model solution. The annual mean transport produced by the pure prognostic calculation for the northwest Atlantic is quite similar to that from the diagnostic calculation in the first year of the simulation, but the model performance deteriorates significantly after the first year. In the second year, for example, the pure prognostic run significantly underestimates the Gulf Stream and North Atlantic Current transports and also incorrectly positions these currents in the model domain. Furthermore, the pure prognostic run does poorly in maintaining the temperature (and therefore density) fronts in the deep waters off the Grand Banks and the Scotian Shelf.

The semiprognostic method improves the performance of the ocean circulation model significantly. It is robust in generating the annual mean transport for each of the 4 years of the model simulation. Of course, some improvement over the purely prognostic results is expected since the model-computed currents in the semiprognostic calculation are adjusted toward the currents produced by diagnostic calculation through the density term in the hydrostatic equation. However, the resulting current estimates are actually a slight improvement over those obtained from the purely diagnostic calculation. These results clearly lend support to the idea that model results can be improved through modifications to the momentum equations without violating conservation principles in the tracer equations.

The most important result produced by the semiprognostic approach is the reliable computation of temperature and salinity evolution, even though the model's temperature and salinity equations are not directly constrained by the semiprognostic procedure. Indeed, the improvement seen in the evolution of the tracers represents the best available validation of the approach taken here and strongly indicates that the approach will be useful in modeling the evolution of tracers other than temperature and salinity that are not so easily observed. The semiprognostic approach might also prove useful as a means of improving the integrity of coupled ocean-atmosphere models. These models often require a "flux correction" procedure to prevent climate drift in the coupled model [e.g., *Manabe and Stouffer*, 1988]. A better representation of the ocean, particularly the temperature field, should enable the flux correction to be reduced or, possibly, even eliminated.

It was noted in section 4 that the pure prognostic calculation does permit mesoscale eddy variability in the model. In the semiprognostic run the mesoscale variability is reduced, although it is not eliminated. This is not surprising because the semiprognostic procedure does introduce damping into the model. The damping effect, however, weakens as the value of α increases. An alternative is to apply the method only on large horizontal scales. Preliminary results suggest that this procedure significantly reduces the damping of the mesoscale variability, but it remains a topic for further study.

Acknowledgments. We wish to thank Youyu Lu, Keith Thompson, Carsten Eden, and two anonymous reviewers for their useful suggestions and comments. J. S. and R. J. G. are supported by the Natural Sciences and Engineering Research Council of Canada (NSERC), MARTEC (a Halifax-based company), and the Meteorological Service of Canada (MSC) through the NSERC/MARTEC/MSC Industrial Research Chair in "Regional Ocean Modelling and Prediction." Financial support for this work has also been received from Canada Foundation for Innovation, the Canadian Institute for Climate Studies, and the Climate Change Action Fund. Current meter data were kindly provided by Doug Gregory of the Bedford Institute of Oceanography.

References

Blumberg, A. F., and G. L. Mellor, A description of a three-dimensional coastal ocean circulation model, in *Three-Dimensional Coastal Ocean Models*, *Coastal Estuarine Stud*., vol. 4, edited by N. S. Heaps, pp. 1–16, AGU, Washington, D. C., 1987.

Csanady, G. T., *Circulation in the Coastal Ocean*, 279 pp., D. Reidel, Norwell, Mass., 1982.

Daley, R., *Atmospheric Data Analysis*, 457 pp., Cambridge Univ. Press, New York, 1991.

da Silva, A. M., C. C. Young, and S. Levitus, *Atlas of Surface Marine Data 1994*, vol. 3, *Anomalies of Heat and Momentum Fluxes*, *NOAA Atlas NESDIS*, vol. 8, 413 pp., Natl. Oceanic Atmos. Assoc., Washington, D. C., 1994.

Dietrich, D. E., Application of a modified Arakawa 'a' grid ocean model having reduced numerical dispersion to the Gulf of Mexico circulation, *Dyn. Atmos. Oceans*, *27*, 201–217, 1997.

Ezer, T., and G. L. Mellor, Diagnostic and prognostic calculations of the North Atlantic circulation and sea level using a sigma coordinate ocean model, *J. Geophys. Res*., *99*, 14,159–14,171, 1994.

Gent, P. R., J. Willebrand, T. J. McDougall, and J. C. McWilliams, Parameterizing eddy-induced tracer transports in ocean circulation models, *J. Phys. Oceanogr*., *25*, 463–474, 1995.

Geshelin, Y., J. Sheng, and R. J. Greatbatch, Monthly mean climatologies of temperature and salinity in the western North Atlantic, *Can. Data Rep. Hydrogr. Ocean Sci*., *153*, 62 pp., 1999.

Ghil, M., Meteorological data assimilation for oceanographers, part I, Description and theoretical framework, *Dyn. Atmos. Oceans*, *13*, 171–218, 1989.

Greatbatch, R. J., Exploring the relationship between eddy-induced transport velocity, vertical momentum transfer and the isopycnal flux of potential vorticity, *J. Phys. Oceanogr*., *28*, 422–432, 1998.

Greatbatch, R. J., and K. G. Lamb, On parameterizing vertical mixing of momentum in non-eddy-resolving ocean models, *J. Phys. Oceanogr*., *20*, 1634–1637, 1990.

Greatbatch, R. J., A. F. Fanning, A. D. Goulding, and S. Levitus, A diagnosis of interpentadal circulation changes in the North Atlantic, *J. Geophys. Res*., *96*, 22,009–22,023, 1991.

Haney, R. L., Surface thermal boundary conditions for ocean circulation models, *J. Phys. Oceanogr*., *1*, 241–248, 1971.

Holloway, G., Representing topographic stress for large-scale ocean models, *J. Phys. Oceanogr*., *22*, 1033–1046, 1992.

Large, W. G., J. C. McWilliams, and S. C. Doney, Oceanic vertical mixing: A review and a model with a nonlocal boundary layer parameterization, *Rev. Geophys*., *32*, 363–403, 1994.

Lazier, J. R. N., and D. G. Wright, Annual velocity variations in the Labrador Current, *J. Phys. Oceanogr*., *23*, 659–678, 1993.

Loder, J. W., B. Petrie, and G. Gawarkiewicz, The coastal ocean off northeastern North America: A large-scale view coastal segment (1, W), *Sea*, *11*, 105–133, 1988.

Manabe, S., and R. J. Stouffer, Two stable equilibria of a coupled ocean-atmosphere model, *J. Clim*., *1*, 841–866, 1988.

Mellor, G. L., C. R. Mechoso, and E. Keto, A diagnostic model of the general circulation of the Atlantic Ocean, *Deep Sea Res*., *Part A*, *29*, 1171–1192, 1982.

Pierce, D. W., Reducing phase and amplitude errors in restoring boundary conditions, *J. Phys. Oceanogr*., *26*, 1552–1560, 1996.

Sarmiento, J. L., and K. Bryan, An ocean transport model for the North Atlantic, *J. Geophys. Res*., *87*, 394–408, 1982.

Sheng, J., D. G. Wright, R. J. Greatbatch, and D. E. Dietrich, CANDIE: A new version of the DieCAST ocean circulation model, *J. Atmos. Oceanic Technol*., *15*, 1414–1432, 1998.

Smagorinsky, J., General circulation experiments with the primitive equation, I, The basic experiment, *Mon. Weather Rev*., *21*, 99–165, 1963.

Smith, P. C., and B. D. Petrie, Low-frequency circulation at the edge of the Scotian Shelf, *J. Phys. Oceanogr*., *12*, 28–46, 1982.

Thuburn, J., Multidimensional flux-limited advection schemes, *J. Comput. Phys*., *123*, 74–83, 1995.

Wardle, R., and J. Marshall, Representation of eddies in primitive equations models by a PV flux, *J. Phys. Oceanogr*., *30*, 2481–2503, 2000.

Webster, F., Vertical profiles of horizontal ocean currents, *Deep Sea Res. Oceanogr. Abstr*., *16*, 85–98, 1969.

Woodgate, R., and P. Killworth, The effect of assimilation on the physics of an ocean model, part I, Theoretical model and barotropic results, *J. Atmos. Oceanic Technol*., *14*, 897–909, 1997.

Wright, D. G., W. P. Connor, and J. Sheng, *CANDIE: A 3D Primitive Equation Model*, *Manual and Model Code*, 69 pp., Bedford Inst. of Oceanogr., Dartmouth, Nova Scotia, 2000.

R. J. Greatbatch and J. Sheng, Department of Oceanography, Dalhousie University, Halifax, Nova Scotia, Canada B3H 4J1. (richard.greatbatch@dal.ca;jinyu.sheng@dal.ca)

D. G. Wright, Fisheries and Oceans Canada, Bedford Institute of Oceanography, Dartmouth, Nova Scotia, Canada B2Y 4A2. (wrightDG@mar.dfo-mpo.gc.ca)

(Received October 25, 2000; revised March 28, 2001;
accepted April 10, 2001.)